ACS OMEGA

http://pubs.acs.org/journal/acsodf

Article

Chitosan Tubes Inoculated with Dental Pulp Stem Cells and Stem Cell Factor Enhance Facial Nerve-Vascularized Regeneration in Rabbits

Xiaodan Mu, Huawei Liu, Shuhui Yang, Yongfeng Li, Lei Xiang, Min Hu,* and Xiumei Wang*

Cite This: *ACS Omega* 2022, 7, 18509−18520

Read Online

ACCESS | Metrics & More | Article Recommendations

ABSTRACT: Facial nerve injury is a common clinical condition that leads to disfigurement and emotional distress in the affected individuals, and the recovery presents clinical challenges. Tissue engineering is the standard method to repair nerve defects. However, nerve regeneration is still not satisfactory because of poor neovascularization after implantation, especially for the long-segment nerve defects. In the current study, we aimed to investigate the potential of chitosan tubes inoculated with stem cell factor (SCF) and dental pulp stem cells (DPSCs) in facial nerve-vascularized regeneration. In the in vitro experiment, DPSCs were isolated, cultured, and then identified. The optimal concentration of SCF was screened by CCK8. Cytoskeleton and living-cell staining, migration, CCK8 test, and neural differentiation assays were performed, revealing that SCF promoted the biological activity of DPSCs. Surprisingly, SCF increased the neural differentiation of DPSCs. The migration and angiogenesis experiments were carried out to show that SCF promoted the angiogenesis and migration of human umbilical vein endothelial cells (HUVECs). In the facial nerve, 7 mm defects of New Zealand white rabbits, hematoxylin−eosin (HE), immunohistochemistry, toluidine blue staining, and transmission electron microscopy observation were performed at 12 weeks postsurgery to show more nerve fibers and better myelin sheath in the SCF + DPSC group. In addition, the whisker movements, Masson's staining, and western blot assays were performed, demonstrating functional repair and that the expression level of CD31 protein in the group SCF + DPSCs was relatively close to that in the group Autograft. In summary, chitosan tubes inoculated with SCF and DPSCs increased neurovascularization and provided an effective method for repairing facial nerve defects, indicating great promise for clinical application.

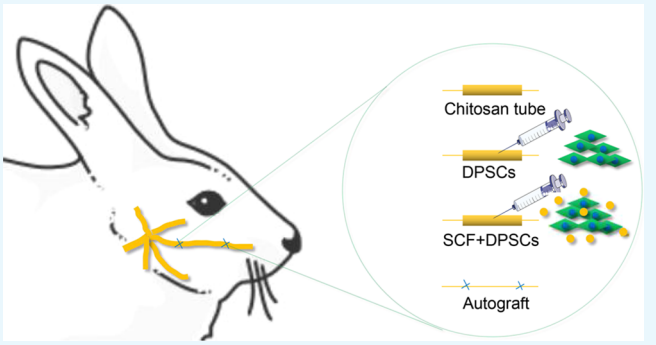

INTRODUCTION

Facial nerve defects severely influence the life quality of patients, especially increasing the psychological burden, and the treatment still faces a substantial clinical challenge.[1−3] Some methods have been used for repairing nerve injury.[4−8] Clinically, the end-to-end coaptation properly repaired the short-gap defect of nerves[9] and difficult to treat the long-gap injury. Currently, the "gold standard" is still autologous nerve transplantation for repairing long-gap nerve defects. However, there are still some problems, including additional surgery, potential cross-infection, lengthy surgical times, lack of host sources, and the mismatches of the nerve length/diameter in donor-recipient.[9−11] Alternatives such as allografts from other humans, nerve conduit,[12−14] biodegradable functionalized materials,[13] neural stem cells, neurotrophic factors,[15] or a combination of the components are efficient in addressing the above-mentioned limitations, but restricted sources present additional issues.[5,16] Novel approaches with similar performance to the Autograft are therefore required for repairing the facial nerve defect.[17]

Stem cells play an increasingly important role in the repair of nerve tissue. Among all kinds of stem cells, dental pulp stem cells (DPSCs), first discovered in the dental pulp tissue,[18] are positive for CD105, CD44, CD73, CD90, and Stro-1.[18−20] In addition, DPSCs are capable of multilineage differentiation, including ectodermal cells (nerve cells), mesodermal cells (odontoblasts, osteoblasts, chondrocytes, and adipocytes), and endodermal cells (insulin-producing cells under appropriate conditions).[18,21−27] Importantly, DPSCs are derived from the neural crest and highly express neural markers such as GFAP,

Received: February 27, 2022
Accepted: May 16, 2022
Published: May 26, 2022

https://doi.org/10.1021/acsomega.2c01176
ACS Omega 2022, 7, 18509−18520

S100, and Nestin.[28] As a result, DPSCs can aid nerve tissue repair and regeneration.

Poor vascularization is one of the reasons behind the regenerated nerves that cannot survive for a long time, leading to a lack of blood supply.[29−31] Therefore, neuro-angiogenesis is vital for the survival of regenerative nerves in the long term. Corresponding to the above point, we selected the stem cell factor (SCF) in the current study. SCF, a glycoprotein dimer (30 kDa) that performs biological activities by interacting with and activating tyrosine kinase c-Kit receptors, is a powerful chemokine. Moreover, SCF has shown excellent potential application prospects because of its homing role in recruiting progenitor cells.[32,33] Currently, SCF has been used in research related to the fertility, normal hematopoiesis, gut movement, pigmentation, and the central nervous system.[34] Furthermore, no studies on the application of SCF in peripheral nerves have been reported. In addition, the relevant literature[35] has shown that SCF (100 ng/mL) promoted the adhesion, activity, proliferation, and migration of DPSCs, which laid a foundation for repairing facial nerve defects by the SCF combined with DPSCs.

Axons can spontaneously regenerate, but the fast-growing connective tissue inhibits the regenerative process.[36] Certainly, the artificial nerve conduit, bridging the two stumps of the defected nerves, provided enough space for nerve regeneration.[8,37] The nerve conduit should have some characteristics, such as sufficient transparency, low tissue adhesion, collapse resistance, and high malleability to facilitate the coaptation of nerve stumps and reduce postoperative complications.[38,39] Several studies have reported that chitosan potentially interacted with the microenvironment related to nerve regeneration, which improved axonal regeneration and reduced neuroma formation.[40−42] The chitosan tube is now commonly employed in the field of peripheral nerve surgery. In addition, recent studies demonstrated that the chitosan tube might be used to regenerate face nerves.[43,44]

In conclusion, the purpose of the current study was to explore the potential of chitosan tubes immersed with stem cell factors and inoculated with dental pulp stem cells to repair the facial nerve. The SCF combined with DPSCs has the potential to provide a new option for the treatment of facial nerve defects.

MATERIALS AND METHODS

DPSCs Isolation and Identification. Dental pulp tissues were removed completely from the intact teeth, digested with collagenase type I for 40 min, neutralized with Dulbecco's modified Eagle medium (DMEM) (10% fetal bovine serum and 1% antibiotic), and cut into pieces (1 mm^3), then inoculated into the dish containing 10% medium. The culture medium was changed every 2 days. All reagents were purchased from Corning.

Immunohistochemical Staining. The cell slides inoculated with DPSCs at a density of 1.5 × 10^4/well were harvested, fixed with 4% formaldehyde, and permeated with Triton-X100 (0.1%). After being treated with 3% H_2O_2 for 15 min and blocked with normal sheep serum, the samples were incubated with primary antibodies against vimentin (Abcam, ab45939, 1:200) and a second antibody (Invitrogen, a48282, 1:400). Next, they were visualized using a DAB chromogenic Kit (Sangon Biotech, PW017) and stained with hematoxylin. Finally, the images were obtained using a bright-field microscope (Leica).

Immunofluorescence Staining. Another cell slide set, also inoculated with DPSCs at the density of 1.5 × 10^4/well and fixed with 4% formaldehyde, was permeated for 20 min with Triton-X100 (0.1%) and incubated with 1% bovine serum albumin (BSA) for 30 min. Then, they were stained with NF200 (Invitrogen, 711025, 1:2500) and Stro-1 (Invitrogen, 14-6688-82, 1:25) at 4 °C overnight, followed by secondary antibody (Invitrogen, a48282, 1:400 and Invitrogen, 31430, 1:5000) for 2 h. After that, the samples were stained with DAPI for 10 min and visualized under a fluorescent microscope.

Alizarin Red Staining. When DPSCs were inoculated on the 24-well plates at a density of 6 × 10^4/well spread up to 80%, and the 10% medium was replaced with the osteogenic medium (DMEM supplemented with 10% FBS, 0.1 mM dexamethasone, 10mMb glycerophosphate, 0.05 mM ascorbate-2-phosphate, 100 U/mL penicillin, 100 mg/mL streptomycin, and 100 U/mL penicillin). The osteogenic medium was changed every two days. Alizarin red staining was carried out to reveal the mineral nodule after 21 days.

Alkaline Phosphatase Staining. When DPSCs were inoculated on the 24-well plates at a density of 7 × 10^4/well spread up to 80%, the 10% medium was replaced with the above-mentioned osteogenic medium. Similarly, the osteogenic medium was changed every two days. Alkaline phosphatase staining was performed according to the instruction of the alkaline phosphatase kit (Sigma Aldrich) after 21 days, revealing the blue−purple precipitate.

SCF Solution Preparation and Screening of the Optimal Concentration. SCF powder (PeproTech) was resuspended in ultrapure water and diluted from the stock (10 mg/mL) to the working solution. DPSCs were digested, centrifuged, and seeded into a 96-well plate with different concentrations (25, 50, 100, 150, and 200 ng/mL) of the SCF at the concentration of 8 × 10^3/mL. There were three replicates in each group. Absorbance values of DPSCs were measured at 460 nm by the CCK8 assay (Dojindo) on the first, fourth, and seventh days. Finally, the optimal concentration was screened.

Cytoskeleton Staining Experiment. DPSCs were inoculated on the cell slides at a density of 1 × 10^4 cells/well, and the SCF was added into the culture medium in the SCF + DPSCs group. The cell slides with or without SCF were collected at 24 h, fixed with 4% paraformaldehyde, permeated by 0.1% Triton-X100, and incubated with rhodamine-labeled phalloidin staining solution (Invitrogen) for 40 min after blocking with 1% BSA and dyed with DAPI (Beyotime). Finally, the images were obtained using confocal fluorescence microscopy (Zeiss LSM 710, Germany; pixel dwell of 2.55 μs, the pinhole aperture of 39 μm, and the lasers were at 488 nm).

Cell Activity Assays. DPSCs were inoculated on the cell slides (1 × 10^5 cells/well). SCF was added to the culture medium in the SCF + DPSCs group. After being washed with PBS, DPSCs were separately dyed for 30 min with calcein AM (Dojindo). Furthermore, the images were photographed using the same microscope equipment described above and were analyzed using the Image J software to count the number of living cells.

Cell Proliferation Assay. DPSCs were inoculated on the cell slides at a density of 8 × 10^3/well, and the SCF was added into the culture medium in the SCF + DPSCs group. There were four multiple pores in each group. Absorbance values of

https://doi.org/10.1021/acsomega.2c01176
ACS Omega 2022, 7, 18509−18520

DPSCs were detected through the CCK8 Kit (according to the instructions) on days 1, 4, and 7.

Cell Migration Assay. DPSCs were inoculated (2×10^4 cells/well) on the transwell insert (nested 24-well plate). Then, 300 μL of the medium was added to the lower chamber. Additionally, SCF was added to the group SCF + DPSCs. After the unmigrated cells were wiped clean, the membrane of the transwell was washed with phosphate buffered saline (PBS), fixed into 4% paraformaldehyde, and dyed with 0.1% crystal violet. Then, using a bright-field microscope (Leica), the unmigrated DPSCs were viewed and photographed. The images were processed using Image J software to count the cells.

Neural Differentiation of DPSCs. DPSCs were inoculated on the cell slides (1.5×10^4 cells/well), and the SCF was added into culture medium in the SCF + DPSCs group. Samples were harvested after being stimulated for 24 h by neurogenic inducing solution I (DMEM/F12 supplemented with 10 ng/mL bFGF, 10% fetal bovine serum, and 500 mM β-mercaptoethanol) and neurogenic inducing solution II (DMEM supplemented with 2% dimethyl sulfoxide and 100 mM butylated hydroxyanisole) for 6 h.[45,46] Then, the samples were fixed in 4% formaldehyde, permeated with Triton-X100 (0.1%) for 20 min, blocked with 1% BSA for 30 min, and stained at 4 °C overnight with NF200 (Invitrogen, 711025, 1:250) and Nestin (Invitrogen, PA5-82905, 1:200). Next, they were incubated with a secondary antibody (Invitrogen, a48282, 1:100) for 2 h. After that, the samples were stained with DAPI for 10 min. The images were photographed using a fluorescent microscope and analyzed using the Image J software for the relative fluorescence area.

Angiogenesis In Vitro Experiment. The angiogenesis experiment of HUVECs was performed as follows: the BD Matrigel was added into the plate (200 μL/well) precooled at 4 °C, and the plate was placed at 37 °C for 30 min. Then, HUVECs were seeded on the surface of Matrigel (2×10^5 cells/well), and the SCF was separately added into the SCF + HUVECs group. The images were collected at 3, 6, and 9 h using an inverted microscope and analyzed using the Image J software for the number of meshes and junctions. Finally, the samples were dyed with calcein AM and photographed again using the fluorescence microscope for easy observation. The migration assay for HUVECs was similar to that described above for DPSCs.

Preparation and Mechanical Properties of the Chitosan Tube. *Preparation of the Chitosan Tube.* The saturated solution was prepared by dissolving the sodium hydroxide powder (Boster) in distilled water. Saturated solution (56 mL) was diluted to 100 mL after clarification. The 3% chitosan solution was used to coat the lumbar puncture needle (21G, Xiyanghong medical equipment, Guangzhou) to ensure a 0.4 mm thickness. Then, the coated needle was inserted into the sodium hydroxide solution (1 mol/L) for 2 min, followed by washing with distilled water, and the chitosan tubes were pulled off the needle and then dried thoroughly. After being cut into 14 mm-long, the chitosan tube was irradiated with cobalt-60 prior to implantation.

Scanning Electron Microscopy Observation. After fixed with 2.5% glutaraldehyde for 30 min, the chitosan tubes were dehydrated through the ethanol gradient and dried by lyophilization. Finally, the tube was sputter-coated with Pt for SEM observation (JEOL, Japan).

Degradation Time. The chitosan tubes were immersed into a lysozyme solution (1 mg/mL) and weighed separately every two weeks until 16 weeks to measure the degradation rate. Five dry chitosan tubes with a length of 14 mm were prepared to measure the quality accurately, immersed in the lysosome solution (1 mg/mL), and then incubated in a 37 °C incubator for 24 h to make the tubes fully swell. The water on the surface of the tubes was absorbed with filter paper, and the samples were weighed again. Then, the swelling coefficient (SI) was calculated according to the formula: (SI (%) = $(W_{wet} \cdot W_{dry})/W_{dry} \times 100\%$, in which W_{dry} and W_{wet} refer to the quality of the tubes before and after swelling, respectively).

Tensile Test. Tensile tests of the chitosan tubes were measured using the Instron universal testing machine (Model 5566). Both ends of the tubes were coated with paraffin adhesive and embedded into the customized cylindrical support equipment. The tubes were fixed on the fixture connected to the test machine. The coupling speed was adjusted to make the tensile speed 5 mm/min.

Animals and Surgical Procedures. The surgical procedure on the rabbits was performed according to Guides for the Care and Use of Laboratory Animals from the Chinese Ministry of Public Health and U.S. National Institutes of Health. Twenty-eight adults New Zealand white rabbits provided by the Animal Laboratory of PLA General Hospital were raised for 1 week to adjust to the laboratory environment. Rabbits with the symmetric autonomous lip-sipping and whisker movements were distributed into four groups (Figure 1) as follows: the chitosan tube group (CST group, $n = 7$), the

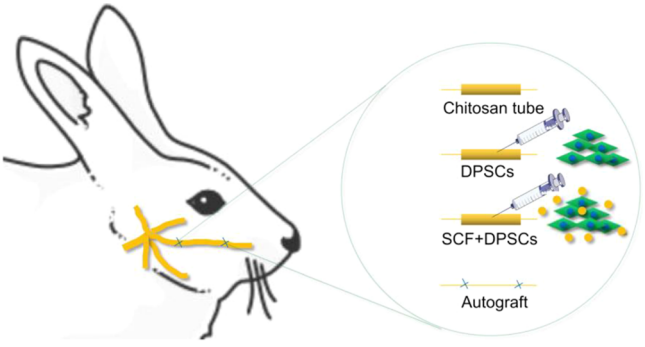

Figure 1. Schematic diagram of nerve graft repairing the buccal branch of the facial nerve in rabbits.

chitosan tube inoculated with dental pulp stem cells (DPSCs group, $n = 7$), the chitosan tubes inoculated with dental pulp stem cells and stem cell factors (SCF + DPSCs group, $n = 7$), and the autografted nerve rotated by a 180° group (Autograft group, $n = 7$). Pentobarbital sodium (35 mg/kg, IV) was used to anesthetize the rabbits, and surgery was conducted after the anesthesia was suitably profound. After the cheek hair removal, the operation area was disinfected with iodoform and covered with a sterile towel. The right buccal branch of the facial nerve was exposed after incision of the skin and subcutaneous tissue. A 7 mm segment was excised under the microsurgery, leaving the 10-mm gaps after nerve ends retracted naturally, which were then bridged with CST, the CST inoculated with DPSCs, the CST inoculated with SCF and DPSCs, and the autografted nerve. When the nerve defect was formed, both nerve ends were inserted separately for 2 mm into the chitosan tube and sutured with the microsutures of 7−0. The rubber plug was placed at both ends to prevent fluid loss. Then, the prepared

https://doi.org/10.1021/acsomega.2c01176
ACS Omega 2022, 7, 18509−18520

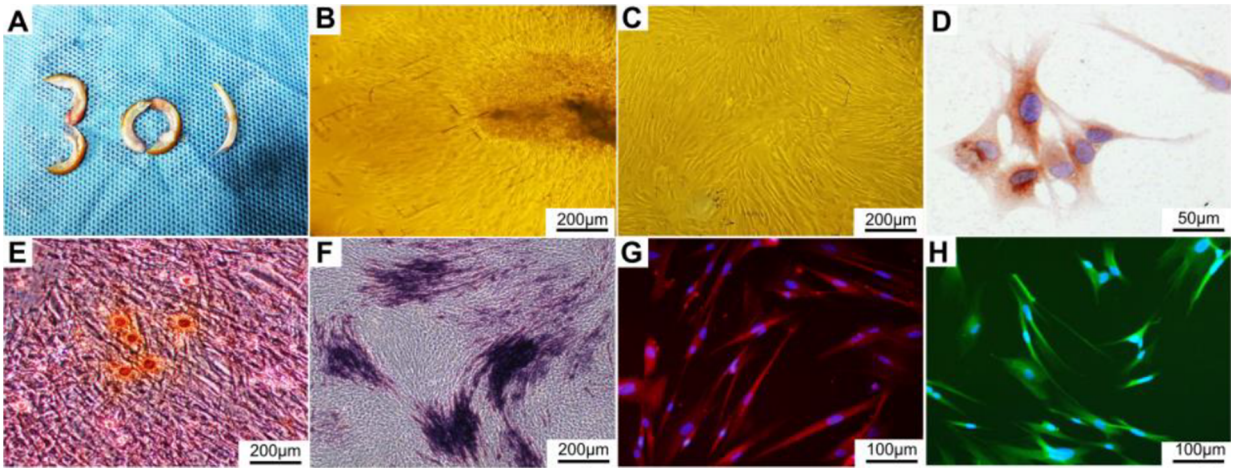

Figure 2. Culture and identification of DPSCs. (A) Teeth of New Zealand white rabbits; (B) primary culture; (C) subculture; (D) immunohistochemical staining of vimentin; (E) alizarin red staining; (F) alkaline phosphatase staining; (G) immunofluorescence staining of NF200 (red); (H) immunofluorescence staining of Stro1 (green).

DPSCs suspension containing SCF was injected into the tubes through microinjection (each injection was of 10uL, with a total of 4 injections). The total number of cells in each group was 3×10^6. After 10 min, the rubber plug was removed, and the muscle and skin were then sutured separately. Furthermore, the rabbits were left to recover for 12 weeks until euthanasia. The experiment was conducted according to the Ethical Review of Laboratory Animal Welfare guidelines (GB/T358922018). The current study was approved and supervised by the Institutional Animal Care and Use Committee of Chinese PLA General Hospital (Beijing, China; approval document no. SQ2022401).

Histomorphological Observation of the Regenerated Facial Nerve. *Immunohistochemical Analysis.* The middle segment of the regenerated nerve was harvested, fixed with 4% formaldehyde, embedded in paraffin, and cut into transverse sections at 3 μm. Moreover, the sections were blocked with serum, stained with primary antibodies against S100 (Invitrogen, MA5-32985, 1:100), neurofilament (Invitrogen, 711025, 1:2000), and hematoxylin and eosin (H&E), then incubated with the second antibody (Invitrogen, a48282, 1:400 and Invitrogen, 31430, 1:5000), and stained with hematoxylin. Finally, the sections were photographed using a bright-field microscope (Leica), and the images were analyzed using the Image J software for the relative area of axons.

Toluidine Blue Staining and TEM Observation. The distal ends of regenerated nerves were fixed with 2.5% glutaraldehyde and 1% osmium tetroxide solution, and dehydrated in a crescent ethanol gradient (50, 70, 80, 90, 95, and 100%). Then, the samples were embedded in epoxy resin, were cut into ultrathin sections (70 nm) for observation under the light microscope (Leica) after staining with 1% toluidine blue and semithin sections (700 nm) for observation by TEM (JEOL, Japan) after staining with uranyl acetate and lead citrate. The images were analyzed using the Image J software for the number of myelinated nerve fibers, the thickness of the myelin sheath, and the diameter of myelinated nerve fibers.

Functional Evaluation of the Regenerated Facial Nerve. *Masson's Trichrome Staining.* At 12 weeks postoperatively, the buccinator muscles harvested from the four groups were fixed in 4% paraformaldehyde. Next, the samples were embedded in paraffin and cut into 7 μm thick sections for Masson's trichrome staining. Finally, the photographs were obtained using the bright-field microscope and analyzed using the Image J software for the area of muscle fibers.

Whisker Movements. Three observers evaluated the whisker movements separately every three weeks according to grading standards: 0 means no apparent movement; 1 means almost imperceptible movement; 2 means fewer significant autonomous movements; 3 means significant but an asymmetric autonomous movement; and 4 means symmetric autonomous movement.[43,45]

Positive Expression of CD31. Four regenerated nerve grafts (CST, DPSCs, SCF + DPSCs, and Autograft) were lysed with RIPA lysate (ProTech) 12 weeks after operation. Then, the protein concentration was detected using a protein assay kit (Bosterbio). Next, the total protein was separated via sodium dodecyl sulfate-polyacrylamide gel electrophoresis (SDS-PAGE) and transferred to the polyvinylidene fluoride (PVDF) membrane preblocked with 5% non-fat milk. Then, the PVDF membrane was incubated with anti-CD31 monoclonal primary antibody (GeneTex, JC70A, 1:100) at 4 °C overnight and incubated with secondary antibody (Invitrogen, 31430, 1:5000) for 1 h. The signals of CD31 were visualized using the hypersensitive ECL chemiluminescence reagent (Boster, AR1171), and the result was analyzed using the Image J software for the relative CD31 protein expression level.

Statistical Analysis. Statistical results were analyzed using the SPSS software. The data were presented in mean ± standard deviation and were analyzed using the independent *t*-test or one-way analysis of variance (ANOVA). Each experiment was performed in triplicate. $P < 0.05$ was considered statistically different.

RESULTS

Culture and Identification of DPSCs. The rabbit incisors are shown in Figure 2A. The cell migrated from around the dental pulp tissue of rabbits approximately 7−10 days after isolation (Figure 2B). DPSCs were then subcultured and presented the typical morphology (the spindle-like shape) (Figure 2C) of mesenchymal stem cells. Moreover, DPSCs expressed vimentin positively after immunohistochemical staining (Figure 2D). In addition, DPSCs showed mineralized

https://doi.org/10.1021/acsomega.2c01176
ACS Omega 2022, 7, 18509−18520

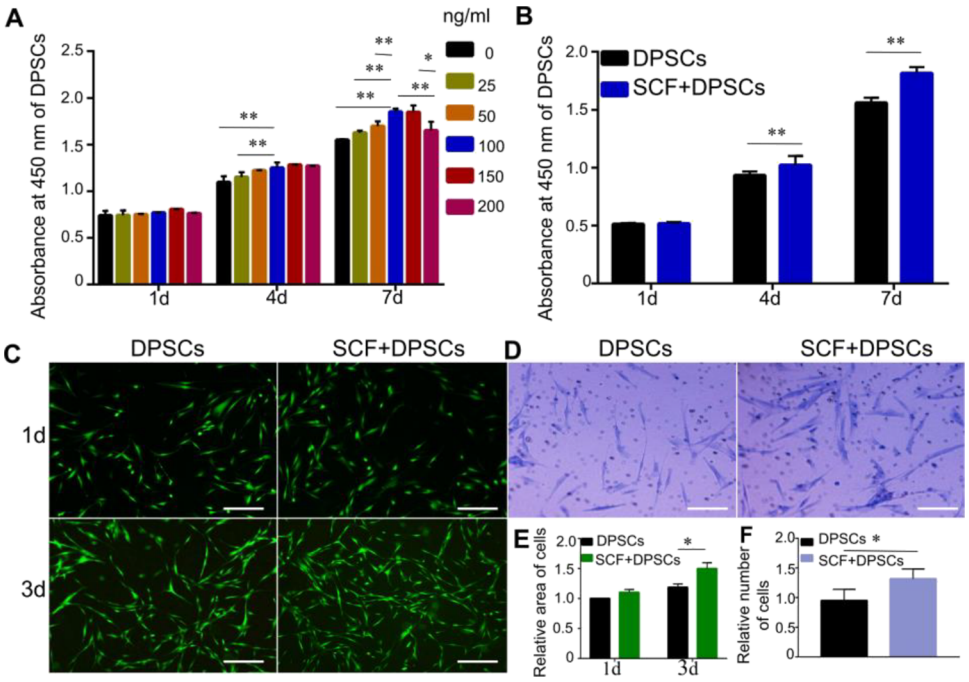

Figure 3. Screening optimal concentration of SCF and the effect of SCF on activity, proliferation, and migration. (A) Screening optimal concentration of SCF; (B) SCF promoted the proliferation and migration of DPSCs; (C) SCF promoted the activity of DPSCs; (D) SCF promoted the migration of DPSCs. (*P < 0.05, **P < 0.01). Scale bar: 200 μm. *P < 0.05, **P < 0.01.

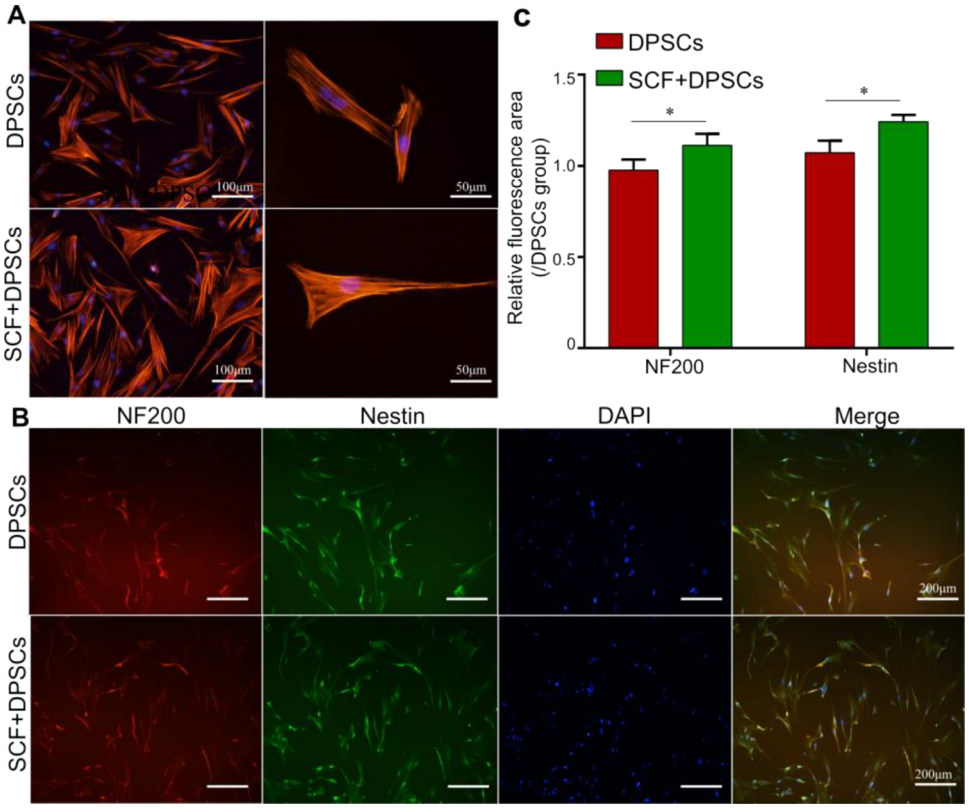

Figure 4. Effect of SCF on skeleton and neural differentiation of DPSCs. (A) SCF promoted skeleton extension; (B) SCF promoted neural differentiation, and corresponding statistical results (C). *P < 0.05, **P < 0.01.

nodules (Figure 2E) and bluish violet precipitate (Figure 2F) by the alizarin red staining and the alkaline phosphatase staining, which indicated the potential of cells for osteogenic differentiation. Furthermore, DPSCs expressed NF200 (Figure 2G) by immunofluorescence staining, which revealed that it had the potential for neurogenic differentiation and expressed Stro-1 (Figure 2H) to show the ability to differentiate. In brief,

https://doi.org/10.1021/acsomega.2c01176
ACS Omega 2022, 7, 18509−18520

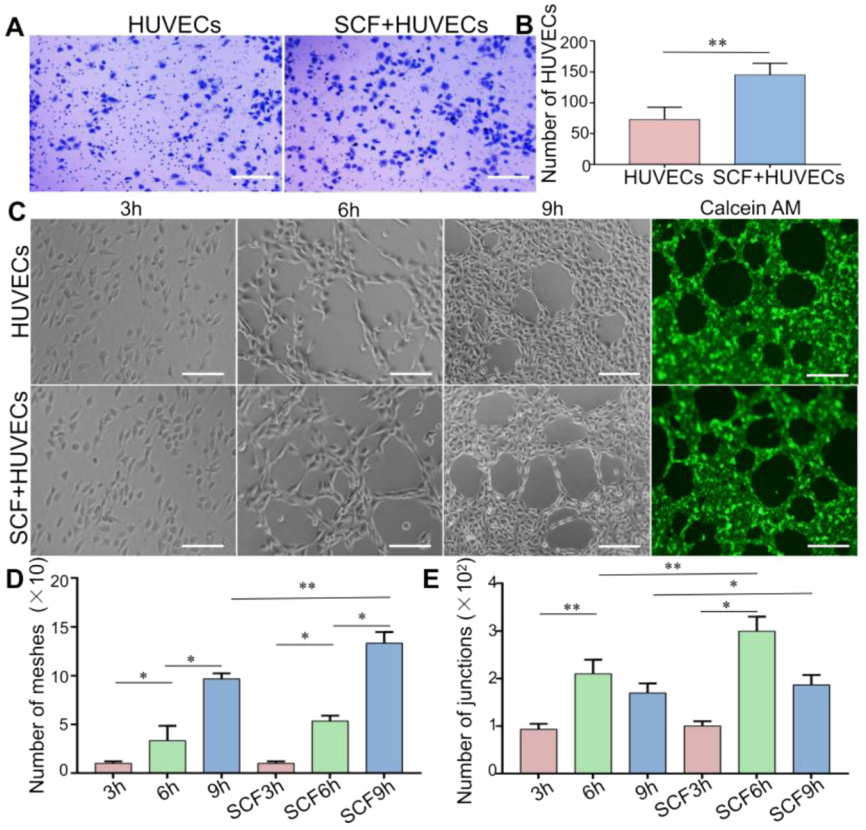

Figure 5. Angiogenesis experiments in vitro. (A) Representative images of migration and the statistical results of migration (B). (C) Vascular-like structures formed in 3, 6, and 9 h, and the vascular-like structures formed in the ninth hour were dyed with calcein AM for easy observation. Statistical results include (D) meshes and (E) junctions. Scale bar: 200 μm. *P < 0.05, **P < 0.01.

the cells isolated from dental pulp tissue for this study can be defined as DPSCs.

Screening the Optimal Concentration of SCF. The absorbance value of the groups with SCF was higher than those without SCF (Figure 3A), showing that SCF increased the proliferation of DPSCs. On day 4, the higher the concentration, the faster the proliferation under 100 ng/mL concentration. When the concentration increased from 150 to 200 ng/mL, the cell number exhibited a downward trend. Also, there were statistical differences between the group 100 ng/mL and the groups 0, 25, and 200 ng/mL (P < 0.01), and not (P > 0.05) between groups 50, 150, and 200 ng/mL. On day 7, there were no significant differences between the groups 100 and 150 ng/mL group (P > 0.05), but there was a significant difference between the groups 100 and 50 ng/mL (P < 0.05). Thus, 100 ng/mL was prepared for the following experiment.

SCF Promoted the Activity, Migration, and Proliferation of DPSCs. The proliferation experiment is shown in Figure 3B. The cell number in the SCF + DPSCs group was obviously more than that in the DPSCs group on days 4 and 7 (P < 0.01) except on day 1 (P > 0.05), which indicates that SCF increased the proliferation of DPSCs. In the living-cell staining experiment (Figure 3C), the group SCF + DPSCs was significantly more than the group DPSCs on day 3(P < 0.01), as shown in the statistical result (Figure 3E), which shows that SCF facilitated the activity of DPSCs. The migration result of DPSCs is shown in Figure 3D. The DPSCs that passed through the transwell in the SCF + DPSCs group were more than those in the DPSC group, as shown in the statistical analysis (P < 0.01) (Figure 3F).

SCF Promoted the Adhesion and Neural Differentiation of DPSCs. Cytoskeletal staining was performed to evaluate the adhesion (Figure 4A). The cell morphology was mostly typically spindle-shaped in the DPSCs group, and the cell morphology was polygonal, and the skeleton was more elongated in the SCF + DPSCs group. Furthermore, the SCF + DPSCs group had more cells than the DPSCs group, matching the living-cell staining results. In the neural differentiation of the DPSC experiment, DPSCs expressed Nestin and NF200 protein positively (Figure 4B) after neural induction, and the statistical result as shown in Figure 4C, which indicated that DPSCs had the potential for neural differentiation. Furthermore, the positive expression of Nestin and NF200 increased in the SCF + DPSCs group, which predicted that SCF promoted neural differentiation.

SCF Promoted the Angiogenesis of HUVECs. The migration result is shown in Figure 5A. The group SCF + DPSCs was more than group DPSCs (P < 0.01) in the cell number passed through the transwell according to the statistical analysis (Figure 5B), which indicated that the SCF facilitated the migration of HUVECs. The vascular-like structures formed at hours 3, 6, and 9 in two groups are shown in Figure 5C. The mesh gradually increased from 3 to 9 h, as shown in Figure 5D. The SCF + HUVECs group was more than the HUVECs group in mesh's number both at hours 6 and 9 (P < 0.01), which indicated that the SCF facilitated the formation of the meshes. Moreover, the junction number increased from 3 to 6 h but decreased at 9 h, as shown in Figure 5E. The SCF + HUVEC group was more than the HUVEC group in the junction's number both at hours 6 and 9

https://doi.org/10.1021/acsomega.2c01176
ACS Omega 2022, 7, 18509−18520

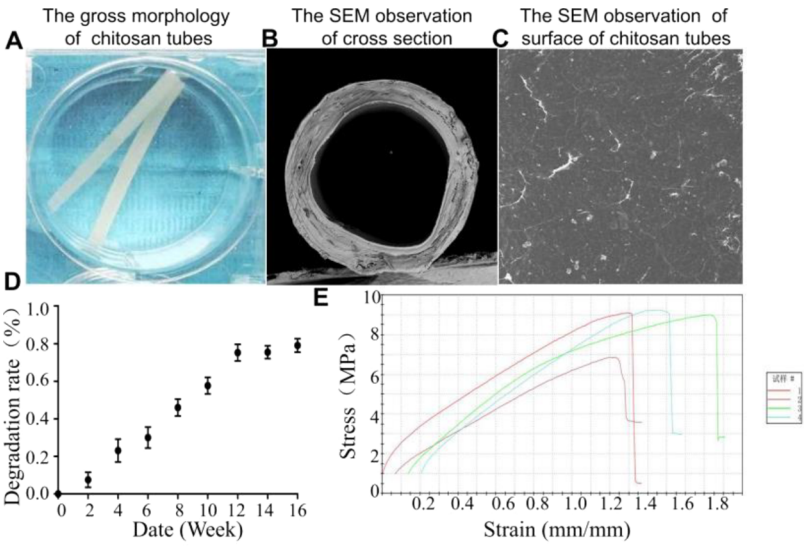

F Swelling and mechanical properties of chitosan tubes (n=4)

Samples	Swelling Index (%)	Elastic modulus (MPa)	Tensile strength (MPa)	Breaking elongation (%)
Chitosan tubes	120.4±3.9	180±40.3	8.6±1.4	8.2±1.8

Figure 6. Mechanical properties of the chitosan tube.

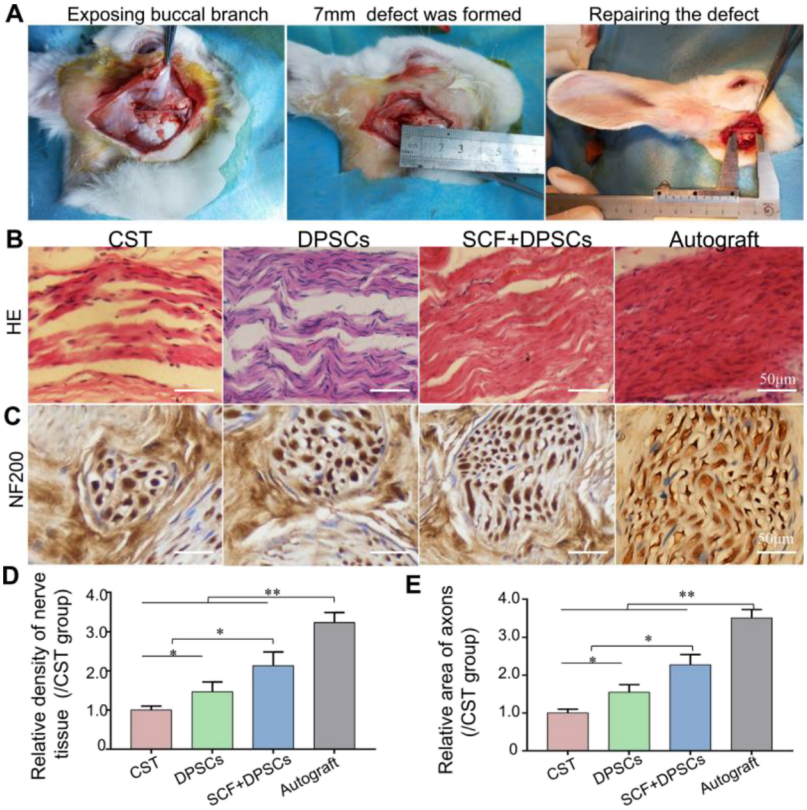

Figure 7. Surgical procedures and evaluation of regenerated facial nerve fibers isolated from the middle of the implants at 12 weeks after surgery. (A) Surgical procedures; (B) hematoxylin−eosin (HE)-stained longitudinal sections and the statistical results (D); (C) immunohistochemical staining and the statistical results (E). (n = 6). *P < 0.05, **P < 0.01.

(P < 0.05), indicating that the SCF increased the formation of junctions.

Mechanical Properties of the Chitosan Tube. The gross morphology of chitosan tubes was translucent (Figure 6A). The chitosan tube maintained its hollow structure, the image of SEM revealed no apparent collapse (Figure 6B), and the surface was smooth (Figure 6C). The degradation rate (Figure 6D) of chitosan tubes increased continuously and

https://doi.org/10.1021/acsomega.2c01176
ACS Omega 2022, 7, 18509−18520

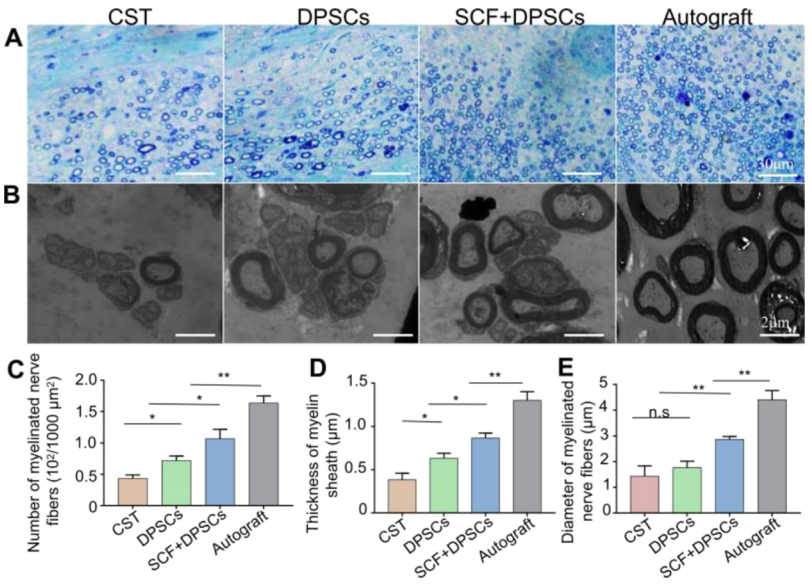

Figure 8. Evaluation of regenerated facial nerve fibers isolated from the distal sections of the implants at 12 weeks after surgery. (A) Toluidine blue-stained transverse sections; (B) TEM images of the regenerated facial nerve. The corresponding statistical results of number of myelinated nerve fibers (C, 10^2/1000 μm^2), the thickness of myelin sheath (D, μm), and the diameter of myelinated nerve fibers (E, μm) (n = 6). *P < 0.05, **P < 0.01.

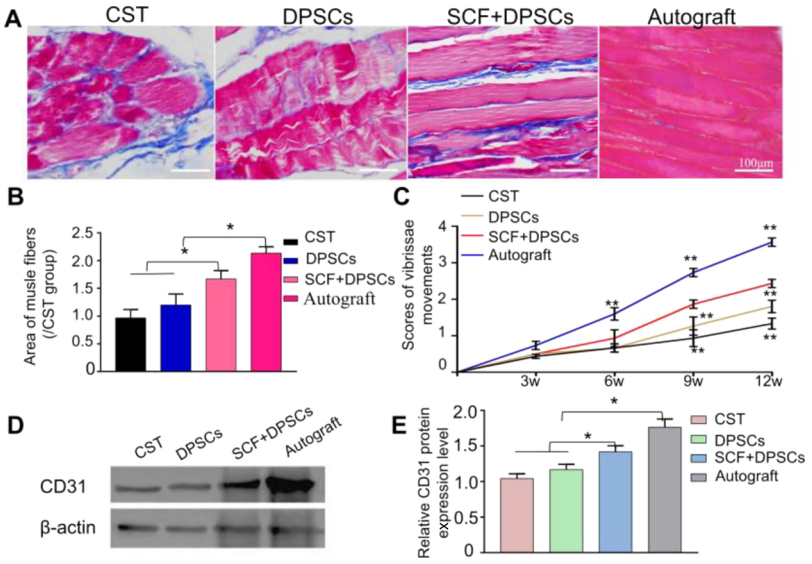

Figure 9. Functional evaluation carried out at 12 weeks after the implantation of regenerated facial nerves. (A) Masson staining of buccal muscles, and the corresponding statistical results (B) (n = 6). (C) Scores of the whisker movement (n = 6). (D) The expression of CD31, and the corresponding statistical results (E).*P < 0.05, **P < 0.01. (n = 3).

reached a stable state in 12 weeks. Furthermore, tensile tests of chitosan tubes were carried out, and the representative diagrams are shown in Figure 6E. The stress of four samples was between 7 and 9 MPa, which indicated that the stress of chitosan tubes was relatively stable and the manufacturing method of chitosan tubes was repeatable. The chitosan tube's mechanical properties analyzed from the tensile test are shown in Figure 6F. The elastic modulus was 180 ± 40.3 MPa, the tensile strength was 8.6 ± 1.4 MPa, and the breaking elongation was 8.2 ± 1.8%, which was consistent with our previous experimental results[43] and meets the mechanical requirements of nerve conduits.[47,48]

SCF + DPSCs Promotes Facial Nerve Regeneration and Remyelination In Vivo. The CST, DPSCs, SCF + DPSCs, and Autograft groups were assessed after bridging 7 mm long gaps of rabbit facial nerves. The main steps of surgical transplantations are shown in Figure 7A. Moreover, no clear neuroma was found when the regenerated facial nerve was harvested at 12 weeks postoperative.

H&E and immunohistochemical staining were carried out 12 weeks after the operation to evaluate the regenerative nerve-like tissue. H&E staining is shown in Figure 7B. The statistical results (Figure 7D) showed that the regenerative nerve-like tissue in the SCF + DPSCs group was relatively close to the Autograft group and obviously more than that in the CST and DPSC groups. The immunohistochemical results of NF200 are shown in Figure 7C. The SCF + DPSCs group was better than the groups DPSCs and CST, and relatively approach the

https://doi.org/10.1021/acsomega.2c01176
ACS Omega 2022, 7, 18509−18520

Autograft group in the nerve diameter. Although, according to the statistical results (Figure 7E), the least positive expression of NF200 was observed in the CST group, followed by the DPSCs group, the expression of NF200 in the SCF + DPSCs group was significantly more than that in both groups above, but lower than in Autograft groups as expected.

Toluidine blue staining (Figure 8A) and TEM (Figure 8B) were performed to evaluate the regenerated axon and remyelination. The more myelinated nerve fibers were observed in the SCF + DPSCs group compared with the CST and DPSCs groups (Figure 8C, $P < 0.01$). The SCF + DPSCs group was thicker than the DPSC and CST groups in the myelin sheath (Figure 8D, $P < 0.05$), and the diameter was also higher in the SCF + DPSCs group (Figure 8E, $P < 0.01$), indicating that SCF + DPSCs exhibited the more apparent effects of facilitation in axonal regeneration and remyelination than DPSCs alone. In addition, the most regenerative facial nerves were found as expected in the Autograft group. The foregoing findings showed that the synergistic action of SCF and DPSCs created a favorable milieu for axon regeneration.

SCF + DPSCs Promotes Functional Recovery of the Regenerated Facial Nerve. Masson's staining of buccal muscle is shown in Figure 9A. The muscle fibers in groups CST and DPSCs were distorted and accompanied by hyperplastic collagen fibers, suggesting that muscles were atrophied to a certain extent. Interestingly, there was a certain amount of collagen fibers in the SCF + DPSCs group. Furthermore, the muscle's morphology in the SCF + DPSCs group approximated to that in the Autograft group, without significant atrophy. The statistical result of muscle fiber's area further proved the better recovery in the AFG + DPSCs and Autograft groups (Figure 9B).

Whisker movement analysis was performed every three weeks, as shown in Figure 9C. Within a week, the whiskers on the surgical side were tilted to the back, and scores of whisker movements decreased to 0, indicating the functional loss of the buccal branch. At week 3, there was no significant difference between the CST, DPSC, and the SCF + DPSCs groups ($P > 0.05$). In the sixth week, the SCF + DPSCs group was slightly higher than the DPSCs and CST groups in the score of whisker movements, but there was no significant difference ($P > 0.05$). At the 9th and 12th weeks, the SCF + DPSCs group's scores were higher than those of the DPSC and CST groups ($P < 0.05$). As expected, the scores of the Autograft were always the highest ($P < 0.01$). Moreover, the score in the SCF + DPSCs group was significantly lower than that in the Autograft group.

Moreover, to explore the vascularization of regenerated facial nerves repaired by SCF + DPSCs, the expression of CD31-associated with the vascular endothelial cell was evaluated by western blot at twelve weeks after transplanting (Figure 9D). The results (Figure 9E) revealed that there was no significant difference in the expression of CD31 between the DPSCs and CST group ($P > 0.05$). Additionally, the CD31 expression in the SCF + DPSCs group was better than the above two groups, relatively close to the Autograft group, indicating SCF promoted facial nerve-vascularized regeneration, which was consistent with the result in vitro.

DISCUSSION

Facial nerve defects reduced the life quality of the affected patients, especially causing psychological burdens of varying degrees. Many scholars are committed to developing the novel approaches with a similar performance to the Autograft for repairing facial nerve injury. The misconnection of nerve fiber and neuroma formation are the common complications of nerve reparation. Because of this, aligned arranged scaffolds have attracted more and more attention and applied to animal experiments for nerve regeneration, but it is still difficult to obtain satisfactory functional recovery. In anatomy, the regeneration of bone tissue is strongly connected to vascularization,[49] and vascularization is very important for dental pulp regeneration in our preliminary work,[35] which prompted us to investigate if vascularization is also very important for nerve regeneration.

The SCF, the important hematopoietic cytokine, was selected in the current study. 100 ng/mL was screened as the optimal concentration, consistent with our previous study,[35] and different from the studies using 50 ng/mL as the optimum concentration of amplification in vitro.[50,51] Furthermore, we hypothesize that the optimal concentration will vary with the cell type. Angiogenesis experiment in vitro demonstrated that the SCF significantly promoted the formation of vascular-like structures and increased the migration of HUVECs, providing a possibility for the facial nerve-vascularized regeneration in the rabbit.

DPSCs, which originated from the neural crest, positively express the marker of nerve cells, differentiate into nerve-like cells, and highly secrete neurotrophic factors.[21,52,53] In addition, the research of Hung and Luo revealed that DPSCs have the properties for vascularization and immunomodulatory properties, which improved neural repair.[54,55] Therefore, DPSCs have the potential to repair nerve defects. In this study, the SCF promoted the migration of DPSCs, which was consistent with a previous study.[51] In addition, in the current investigation, SCF enhanced adhesion, activity, and proliferation, which was favorable for SCF study in combination with DPSCs for tissue regeneration. Surprisingly, the SCF + DPSCs group was more than the DPSCs group in the expression of NF200 and nestin, indicating that the SCF promoted neural differentiation and further increased the potential of the SCF combined with DPSCs for repairing the neural tissue.

In in vivo trials, the facial nerve was repaired using an empty chitosan tube as a negative control, and the regenerated nerve was extremely restricted. The implantation of DPSCs promoted nerve regeneration and myelination in the CST group, showing the potential of DPSCs to repair the peripheral nerve, consistent with the results of studies.[56−59] It is still necessary to add the content related to comparing other cell types with DPSCs in repairing facial nerves to verify further the potential of DPSCs, which will be designed for subsequent research work. The combined implantation of the SCF and DPSCs further promoted regeneration and myelination of nerve fibers and improved the functional recovery, relatively approaching the Autograft group, showing the potential of a synergistic effect of the SCF and DPSCs for repairing the facial nerve. The ultimate aim for peripheral nerve regeneration is the functional recovery of nerve conduction and the predomination of target organs.[60] The structure and function of the buccinator reflect the nerve regeneration degree of the facial nerve buccal branch. Interestingly, there was a certain amount of collagen fibers in the group SCF + DPSCs, and the muscle's morphology approximated to the group Autograft, without significant atrophy. Undoubtedly, the result in the Autograft group was always the best, perhaps because autologous nerve transplantation saved the time for axonal

https://doi.org/10.1021/acsomega.2c01176
ACS Omega 2022, 7, 18509−18520

regeneration and myelination. In addition, allogeneic cells were used to repair facial nerve defects in this study, which largely avoids immune rejection compared to xenogeneic cells.[61] In Wang's study, a 6 mm crush injury of the rat sciatic nerve was successfully repaired by human DPSCs, but xenogeneic cells are challenging to establish a cell repertoire. Given the potential for similar technologies to lower xenogeneic cell immunogenicity and the comparatively restricted supply of human DPSCs compared to animals, xenogeneic cells may be viable for nerve restoration in clinical applications. Furthermore, the survival of DPSCs and the leaking of the SCF should be taken into account. Although the rubber plug at both ends of the tube prevented the loss of cells and factors, there was no direct evidence to prove the number of surviving cells in the in vivo experiment. Thus, the transplantation of fluorescently labeled DPSCs is indispensable to definite the survival of DPSCs. In addition, the sustained-release experiment of the SCF in vitro will contribute to exploring the release of the SCF in vivo.

Although many studies have achieved the repair effects of facial nerves through preclinical models,[62] a few related studies have focused on the vascular regeneration of regenerative nerves. However, tissue regeneration accompanied by angiogenesis is essential for the survival of regenerated tissue.[63] To explore the vascularization of regenerated facial nerve harvested from the SCF + DPSCs group, the expression of CD31 associated with the vascular endothelial cell was assessed by western blot at 12 weeks after the operation. The SCF + DPSCs group was significantly higher than the DPSCs and CST groups and reduced compared to the Autograft group in the expression of CD31, indicating SCF combined with DPSCs promoted facial nerve-vascularized regeneration, which was consistent with the result in vitro and verified that pluripotent cells could increase functional recovery and revascularization in Assis's study.[64] At 12 weeks postoperatively, the chitosan tube protecting the regenerated facial nerve was surrounded by connective tissue containing vascular structures. This connective tissue was not easy to peel off, which affected the positive expression CD31 to some extent. Therefore, this assay still needs to be verified by further experiments.

There are also limitations in the current study. The first is the limited time point of animal sampling. The specimens were only harvested at 12 weeks postoperatively for observation in this study. The time point in actions of SCF and DPSCs maybe defined if the postoperative sampling at 2, 4, 6, 8, and 10 weeks was increased, which is expected to explore the mechanism of SCF and DPSCs in promoting nerve regeneration. The second constraint is the lack of an aligned filler, such as aligned fibrin nanofiber hydrogel,[65] which offers scaffolding for DPSCs and SCF and directs the migration of regenerated nerve fibers to the distal end. The gap with the autologous nerve transplant may be narrowed if the aligned fibrin nanofiber hydrogel inoculated with DPSCs and SCF were helpful in repairing the facial nerve defect. Accordingly, the more models in vivo are essential and very important to be able to translate the achievements to human medicine from one health perspective.[66,67]

CONCLUSIONS

We first proposed the SCF for repairing the peripheral nerve defect in the present study. The SCF promoted the adhesion, activity, proliferation, and migration, especially the neural differentiation of DPSCs, and promoted the neurovascular regeneration. The synergistic effect of SCF and DPSCs resulted in improvements in the facial neurovascular regeneration in this study, reflecting more superiority in repairing nerve defects.

AUTHOR INFORMATION

Corresponding Authors

Min Hu − *Department of Stomotology, The First Medical Centre, Chinese PLA General Hospital, Beijing 100853, China*; Email: humin48@vip.163.com

Xiumei Wang − *Department of Materials Science and Engineering, State Key Laboratory of New Ceramics and Fine Processing, Tsinghua University, Beijing 100084, China*; orcid.org/0000-0002-5303-0217; Email: wxm@mail.tsinghua.edu.cn

Authors

Xiaodan Mu − *Department of Stomotology, The First Medical Centre, Chinese PLA General Hospital, Beijing 100853, China*; orcid.org/0000-0002-2938-2853

Huawei Liu − *Department of Stomotology, The First Medical Centre, Chinese PLA General Hospital, Beijing 100853, China*

Shuhui Yang − *Department of Materials Science and Engineering, State Key Laboratory of New Ceramics and Fine Processing, Tsinghua University, Beijing 100084, China*; orcid.org/0000-0002-8013-1873

Yongfeng Li − *Department of Stomotology, The First Medical Centre, Chinese PLA General Hospital, Beijing 100853, China*

Lei Xiang − *Department of Stomotology, The First Medical Centre, Chinese PLA General Hospital, Beijing 100853, China*

Complete contact information is available at: https://pubs.acs.org/10.1021/acsomega.2c01176

Notes

The authors declare no competing financial interest.

ACKNOWLEDGMENTS

This research was supported by the National key research and development program (2017YFB1104103 and 2017YFA0104700) and the National Natural Science Foundation of China (No. 8190032661). All the authors have given final approval and agreed to be responsible for all aspects of the work.

REFERENCES

(1) Ma, F.; Xu, F.; Li, R.; Zheng, Y.; Wang, F.; Wei, N.; Zhong, J.; Tang, Q.; Zhu, T.; Wang, Z.; Zhu, J. Sustained delivery of glial cell-derived neurotrophic factors in collagen conduits for facial nerve regeneration. *Acta Biomater.* **2018**, *69*, 146−155.

(2) Shafaiee, Y.; Shahbazzadegan, B. Facial Nerve Laceration and its Repair. *Trauma Mon.* **2016**, *21*, No. e22066.

(3) Spector, J. G.; Lee, P.; Derby, A. Rabbit facial nerve regeneration in autologous nerve grafts after antecedent injury. *Laryngoscope.* **2000**, *110*, 660−667.

(4) Carvalho, C. R.; Wrobel, S.; Meyer, C.; Brandenberger, C.; Cengiz, I. F.; López-Cebral, R.; Silva-Correia, J.; Ronchi, G.; Reis, R. L.; Grothe, C.; Oliveira, J. M.; Haastert-Talini, K. Gellan Gum-based luminal fillers for peripheral nerve regeneration: an in vivo study in the rat sciatic nerve repair model. *Biomater. Sci.* **2018**, *6*, 1059−1075.

(5) Ray, W. Z.; Mackinnon, S. E. Management of nerve gaps: autografts, allografts, nerve transfers, and end-to-side neurorrhaphy. *Exp. Neurol.* **2010**, *223*, 77−85.
(6) Zhao, Y.; Liang, Y.; Ding, S.; Zhang, K.; Mao, H. Q.; Yang, Y. Application of conductive PPy/SF composite scaffold and electrical stimulation for neural tissue engineering. *Biomaterials* **2020**, *255*, No. 120164.
(7) Zhan, X.; Gao, M.; Jiang, Y.; Zhang, W.; Wong, W. M.; Yuan, Q.; Su, H.; Kang, X.; Dai, X.; Zhang, W.; Guo, J.; Wu, W. Nanofiber scaffolds facilitate functional regeneration of peripheral nerve injury. *Nanomedicine* **2013**, *9*, 305−315.
(8) Faroni, A.; Mobasseri, S. A.; Kingham, P. J.; Reid, A. J. Peripheral nerve regeneration: experimental strategies and future perspectives. *Adv. Drug Deliv. Rev.* **2015**, *82-83*, 160−167.
(9) Greene, J. J.; McClendon, M. T.; Stephanopoulos, N.; Álvarez, Z.; Stupp, S. I.; Richter, C. P. Electrophysiological assessment of a peptide amphiphile nanofiber nerve graft for facial nerve repair. *J. Tissue. Eng. Regen. Med.* **2018**, *12*, 1389−1401.
(10) Ichihara, S.; Inada, Y.; Nakamura, T. Artificial nerve tubes and their application for repair of peripheral nerve injury: an update of current concepts. *Injury* **2008**, *39*, 29−39.
(11) Sun, Y.; Li, W.; Wu, X.; Zhang, N.; Zhang, Y.; Ouyang, S.; Song, X.; Fang, X.; Seeram, R.; Xue, W.; He, L.; Wu, W. Functional Self-Assembling Peptide Nanofiber Hydrogels Designed for Nerve Degeneration. *ACS. Appl. Mater. Interfaces* **2016**, *8*, 2348−2359.
(12) Stocco, E.; Barbon, S.; Lamanna, A.; de Rose, E.; Zamuner, A.; Sandrin, D.; Marsotto, M.; Auditore, A.; Messina, G. M. L.; Licciardello, A.; Iucci, G.; Macchi, V.; de Caro, R.; Dettin, M.; Porzionato, A. Bioactivated Oxidized Polyvinyl Alcohol towards Next-Generation Nerve Conduits Development. *Polymers (Basel)* **2021**, *13*, 3372.
(13) Sasaki, R.; Watanabe, Y.; Yamato, M.; Okamoto, T. Tissue-engineered nerve guides with mesenchymal stem cells in the facial nerve regeneration. *Neurochem. Int.* **2021**, *148*, No. 105062.
(14) Porzionato, A.; Barbon, S.; Stocco, E.; Dalzoppo, D.; Contran, M.; de Rose, E.; Parnigotto, P. P.; Macchi, V.; Grandi, C.; de Caro, R. Development of Oxidized Polyvinyl Alcohol-Based Nerve Conduits Coupled with the Ciliary Neurotrophic Factor. *Materials (Basel)* **2019**, *12*, 1996.
(15) Barbon, S.; Stocco, E.; Negro, A.; Dalzoppo, D.; Borgio, L.; Rajendran, S.; Grandi, F.; Porzionato, A.; Macchi, V.; de Caro, R.; Parnigotto, P. P.; Grandi, C. In vitro assessment of TAT-Ciliary Neurotrophic Factor therapeutic potential for peripheral nerve regeneration. *Toxicol. Appl. Pharmacol.* **2016**, *309*, 121−128.
(16) Hu, M.; Zhang, L.; Niu, Y.; Xiao, H.; Tang, P.; Wang, Y. Repair of whole rabbit facial nerve defects using facial nerve allografts. *J. Oral. Maxillofac. Surg.* **2010**, *68*, 2196−2206.
(17) Vasconcelos, B. C.; Gay-Escoda, C. Facial nerve repair with expanded polytetrafluoroethylene and collagen conduits: an experimental study in the rabbit. *J. Oral. Maxillofac. Surg.* **2000**, *58*, 1257−1262.
(18) Gronthos, S.; Mankani, M.; Brahim, J.; Robey, P. G.; Shi, S. Postnatal human dental pulp stem cells (DPSCs) in vitro and in vivo. *Proc. Natl. Acad. Sci. U. S. A.* **2000**, *97*, 13625−13630.
(19) Carnevale, G.; Riccio, M.; Pisciotta, A.; Beretti, F.; Maraldi, T.; Zavatti, M.; Cavallini, G. M.; la Sala, G. B.; Ferrari, A.; de Pol, A. In vitro differentiation into insulin-producing β-cells of stem cells isolated from human amniotic fluid and dental pulp. *Dig. Liver Dis.* **2013**, *45*, 669−676.
(20) Sakai, K.; Yamamoto, A.; Matsubara, K.; Nakamura, S.; Naruse, M.; Yamagata, M.; Sakamoto, K.; Tauchi, R.; Wakao, N.; Imagama, S.; Hibi, H.; Kadomatsu, K.; Ishiguro, N.; Ueda, M. Human dental pulp-derived stem cells promote locomotor recovery after complete transection of the rat spinal cord by multiple neuro-regenerative mechanisms. *J. Clin. Invest.* **2012**, *122*, 80−90.
(21) Arthur, A.; Rychkov, G.; Shi, S.; Koblar, S. A.; Gronthos, S. Adult human dental pulp stem cells differentiate toward functionally active neurons under appropriate environmental cues. *Stem Cells* **2008**, *26*, 1787−1795.
(22) Monteiro, B. G.; Serafim, R. C.; Melo, G. B.; Silva, M. C. P.; Lizier, N. F.; Maranduba, C. M. C.; Smith, R. L.; Kerkis, A.; Cerruti, H.; Gomes, J. A. P.; Kerkis, I. Human immature dental pulp stem cells share key characteristic features with limbal stem cells. *Cell Prolif.* **2009**, *42*, 587−594.
(23) Iohara, K.; Zheng, L.; Ito, M.; Tomokiyo, A.; Matsushita, K.; Nakashima, M. Side poplation cells isolated from porcine dental pulp tissue with self-renewal and multipotency for detingenesis, chondrogenesis, and neurongenesis. *Stem Cells* **2006**, *24*, 2493−2503.
(24) Pierdomenico, L.; Bonsi, I.; Calvitti, M.; Rondelli, D.; Arpinati, M.; Chirumbolo, G.; Becchetti, E.; Marchionni, C.; Alviano, F.; Fossati, V.; Staffolani, N.; Franchina, M.; Grossi, A.; Bagnara, G. P. Multipotent mesenchymal stem cells with immunosuppressive activity can be easily isolated from dental pulp. *Transplantation* **2005**, *80*, 836−842.
(25) Zhang, W.; Walboomers, X. F.; Shi, S.; Fan, M.; Jansen, J. A. Multilineage differentiation potential of stem cells derived from human dental pulp after cryopreservaton. *Tissue Eng.* **2006**, *12*, 2813−2823.
(26) Gronthos, S.; Brahim, J.; Li, W.; Fisher, L. W.; Cherman, N.; Boyde, A.; DenBesten, P.; Robey, P. G.; Shi, S. Stem cell properties of human dental pulp cells. *J. Dent. Res.* **2002**, *81*, 531−535.
(27) Siqueira da Fonseca, S. A.; Abdelmassih, S.; de Mello Cintra Lavagnolli, T.; Serafim, R. C.; Clemente Santos, E. J.; Mota Mendes, C.; de Souza Pereira, V.; Ambrosio, C. E.; Miglino, M. A.; Visintin, J. A.; Abdelmassih, R.; Kerkis, A.; Kerkis, I. Human immature dental pulp stem cells contribution to developing mouse embryos:Production of human/mouse preterm chiameras. *Cell Prolif.* **2009**, *42*, 132−140.
(28) Yamamoto, A.; Sakai, K.; Matsubara, K.; Kano, F.; Ueda, M. Multifaceted neuro-regenerative activities of human dental pulp stem cells for functional recovery after spinal cord injury. *Neurosci. Res.* **2014**, *78*, 16−20.
(29) Konofaos, P.; ver Halen, J. Nerve repair by means of tubulization: past, present, future. *J. Reconstr. Microsurg.* **2013**, *29*, 149−164.
(30) Bueno, F. R.; Shah, S. B. Implications of tensile loading for the tissue engineering of nerves. *Tissue Eng. Part B. Rev.* **2008**, *14*, 219−233.
(31) Huang, L.; Zhu, L.; Shi, X.; Xia, B.; Liu, Z.; Zhu, S.; Yang, Y.; Ma, T.; Cheng, P.; Luo, K.; Huang, J.; Luo, Z. A compound scaffold with uniform longitudinally oriented guidance cues and a porous sheath promotes peripheral nerve regeneration in vivo. *Acta Biomater.* **2018**, *68*, 223−236.
(32) Liu, X.; Wang, X.; Wang, X.; Ren, H.; He, J.; Qiao, L.; Cui, F. Z. Functionalized self-assembling peptide nanofiber hydrogels mimic stem cell niche to control human adipose stem cell behavior in vitro. *Acta Biomater.* **2013**, *9*, 6798−6805.
(33) Kisiday, J.; Jin, M.; Kurz, B.; Hung, H.; Semino, C.; Zhang, S.; Grodzinsky, A. J. Self-assembling peptide hydrogel fosters chondrocyte extracellular matrix production and cell division: implications for cartilage tissue repair. *Proc. Natl. Acad. Sci. U. S. A.* **2002**, *99*, 9996−10001.
(34) Lennartsson, J.; Rönnstrand, L. Stem cell factor receptor/c-Kit: from basic science to clinical implications. *Physiol. Rev.* **2012**, *92*, 1619−1649.
(35) Mu, X. D.; Shi, L.; Pan, S.; He, L. N.; Niu, Y. M.; Wang, X. M. A Customized Self-Assembling Peptide Hydrogel Wrapped Stem Cell Factor Targeting Pulp Regeneration Rich in Vascular-Like Structures. *ACS Omega* **2020**, *5*, 16568−16574.
(36) Uz, M.; Sharma, A. D.; Adhikari, P.; Sakaguchi, D. S.; Mallapragada, S. K. Development of multifunctional films for peripheral nerve regeneration. *Acta Biomater.* **2017**, *56*, 141−152.
(37) Gu, X.; Ding, F.; Williams, D. F. Neural tissue engineering options for peripheral nerve regeneration. *Biomaterials* **2014**, *35*, 6143−6156.
(38) Sarker, M. D.; Naghieh, S.; McInnes, A. D.; Schreyer, D. J.; Chen, X. Regeneration of peripheral nerves by nerve guidance

https://doi.org/10.1021/acsomega.2c01176
ACS Omega 2022, 7, 18509−18520

conduits: Influence of design, biopolymers, cells, growth factors, and physical stimuli. *Prog. Neurobiol.* **2018**, *171*, 125−150.
(39) Alvites, R. D.; Branquinho, M. V.; Sousa, A. C.; Amorim, I.; Magalhães, R.; João, F.; Almeida, D.; Amado, S.; Prada, J.; Pires, I.; Zen, F.; Raimondo, S.; Luís, A. L.; Geuna, S.; Varejão, A. S. P.; Maurício, A. C. Combined Use of Chitosan and Olfactory Mucosa Mesenchymal Stem/Stromal Cells to Promote Peripheral Nerve Regeneration In Vivo. *Stem Cells Int.* **2021**, *2021*, 13029.
(40) Boecker, A.; Daeschler, S. C.; Kneser, U.; Harhaus, L. Relevance and Recent Developments of Chitosan in Peripheral Nerve Surgery. *Front. Cell. Neurosci.* **2019**, *13*, 104.
(41) Zhao, Y.; Wang, Y.; Gong, J.; Yang, L.; Niu, C.; Ni, X.; Wang, Y.; Peng, S.; Gu, X.; Sun, C.; Yang, Y. Chitosan degradation products facilitate peripheral nerve regeneration by improving macrophage-constructed microenvironments. *Biomaterials* **2017**, *134*, 64−77.
(42) Younes, I.; Rinaudo, M. Chitin and Chitosan Preparation from Marine Sources. Structure, Properties and Applications. *Mar. Drugs* **2015**, *13*, 1133−1174.
(43) Mu, X. D.; Sun, X. Y.; Yang, S. S.; Pan, S.; Sun, J. X.; Niu, Y. M.; He, L. N.; Wang, X. M. Chitosan Tubes Prefilled with Aligned Fibrin Nanofiber Hydrogel Enhance Facial Nerve Regeneration in Rabbits. *ACS Omega* **2021**, *6*, 26293−26301.
(44) Liu, H.; Wen, W.; Hu, M.; Bi, W.; Chen, L.; Liu, S.; Chen, P.; Tan, X. Chitosan conduits combined with nerve growth factor microspheres repair facial nerve defects. *Neural Regen. Res.* **2013**, *8*, 3139−3147.
(45) Black, I. B.; Woodbury, D. Adult rat and human bone marrow stromal stem cells differentiate into neurons. *Blood Cells Mol Dis.* **2001**, *27*, 632−636.
(46) Woodbury, D.; Schwarz, E. J.; Prockop, D. J.; Black, I. B. Adult rat and human bone marrow stromal cells differentiate into neurons. *J. Neurosci. Res.* **2000**, *61*, 364−370.
(47) Cao, W.; Cheng, M.; Ao, Q.; Gong, Y.; Zhao, N.; Zhang, X. Physical, mechanical and degradation properties, and schwann cell affinity of cross-linked chitosan films. *J. Biomater. Sci. Polym. Ed.* **2005**, *16*, 791−807.
(48) Wenling, C.; Duohui, J.; Jiamou, L.; Yandao, G.; Nanming, Z.; Xiufang, Z. Effects of the degree of deacetylation on the physicochemical properties and Schwann cell affinity of chitosan films. *J. Biomater. Appl.* **2005**, *20*, 157−177.
(49) Zha, Y.; Li, Y.; Lin, T.; Chen, J.; Zhang, S.; Wang, J. Progenitor cell-derived exosomes endowed with VEGF plasmids enhance osteogenic induction and vascular remodeling in large segmental bone defects. *Theranostics.* **2021**, *11*, 397−409.
(50) Zheng, Y.; Sun, A.; Han, Z. C. Stem cell factor improves SCID-repopulating activity of human umbilical cord blood-derived hematopoietic stem/progenitor cells in xenotransplanted NOD/SCID mouse model. *Bone Marrow Transplant.* **2005**, *35*, 137−142.
(51) Pan, S.; Dangaria, S.; Gopinathan, G.; Yan, X.; Lu, X.; Kolokythas, A.; Niu, Y.; Luan, X. SCF promotes dental pulp progenitor migration, neovascularization, and collagen remodeling - potential applications as a homing factor in dental pulp regeneration. *Stem Cell Rev. Rep.* **2013**, *9*, 655−667.
(52) Karaöz, E.; Demircan, P. C.; Sağlam, Ö.; Aksoy, A.; Kaymaz, F.; Duruksu, G. Human dental pulp stem cells demonstrate better neural and epithelial stem cell properties than bone marrow-derived mesenchymal stem cells. *Histochem. Cell Biol.* **2011**, *136*, 455−473.
(53) Mead, B.; Logan, A.; Berry, M.; Leadbeater, W.; Scheven, B. A. Paracrine-mediated neuroprotection and neuritogenesis of axotomised retinal ganglion cells by human dental pulp stem cells: comparison with human bone marrow and adipose-derived mesenchymal stem cells. *PLoS One* **2014**, *9*, No. e109305.
(54) Tran-Hung, L.; Laurent, P.; Camps, J.; About, I. Quantification of angiogenic growth factors released by human dental cells after injury. *Arch. Oral Biol.* **2008**, *53*, 9−13.
(55) Luo, L.; Albashari, A. A.; Wang, X.; Jin, L.; Zhang, Y.; Zheng, L.; Xia, J.; Xu, H.; Zhao, Y.; Xiao, J.; He, Y.; Ye, Q. Effects of Transplanted Heparin-Poloxamer Hydrogel Combining Dental Pulp Stem Cells and bFGF on Spinal Cord Injury Repair. *Stem Cells Int.* **2018**, *2018*, 1−13.
(56) Wang, D. R.; Wang, Y. H.; Pan, J.; Tian, W. D. Neurotrophic effects of dental pulp stem cells in repair of peripheral nerve after crush injury. *World J. Stem Cells.* **2020**, *12*, 1196−1213.
(57) Takaoka, S.; Uchida, F.; Ishikawa, H.; Toyomura, J.; Ohyama, A.; Watanabe, M.; Matsumura, H.; Marushima, A.; Iizumi, S.; Fukuzawa, S.; Ishibashi-Kanno, N.; Yamagata, K.; Yanagawa, T.; Matsumaru, Y.; Bukawa, H. Transplanted neural lineage cells derived from dental pulp stem cells promote peripheral nerve regeneration. *Hum. Cell* **2022**, *35*, 462−471.
(58) Mohan, S. P.; Ramalingam, M. Dental Pulp Stem Cells in Neuroregeneration. *J. Pharm. Bioallied Sci.* **2020**, *12*, S60−S66.
(59) Sasaki, R.; Aoki, S.; Yamato, M.; Uchiyama, H.; Wada, K.; Okano, T.; Ogiuchi, H. Tubulation with Dental Pulp Cells Promotes Facial Nerve Regeneration in Rats. *Tissue Eng. Part A.* **2008**, *14*, 1141−1147.
(60) Santos Roballo, K. C.; Dhungana, S.; Jiang, Z.; Oakey, J.; Bushman, J. S. Localized delivery of immunosuppressive regulatory T cells to peripheral nerve allografts promotes regeneration of branched segmental defects. *Biomaterials* **2019**, *209*, 1−9.
(61) Saez, D. M.; Sasaki, R. T.; Martins, D. O.; Chacur, M.; Kerkis, I.; da Silva, M. C. P. Rat Facial Nerve Regeneration with Human Immature Dental Pulp Stem Cells. *Cell Transplant.* **2019**, *28*, 1573−1584.
(62) Bengur, F. B.; Stoy, C.; Binko, M. A.; Nerone, W. V.; Fedor, C. N.; Solari, M. G.; Marra, K. G. Facial Nerve Repair: Bioengineering Approaches in Preclinical Models. *Tissue Eng. Part B. Rev.* **2022**, *28*, 364−378.
(63) Wei, Y.; Wang, F.; Guo, Z.; Zhao, Q. Tissue-engineered vascular grafts and regeneration mechanisms. *J. Mol. Cell. Cardiol.* **2022**, *165*, 40−53.
(64) de Assis, A. C. C.; Reis, A.; Nunes, L. V., Ferreira, L. F. R., Bilal, M., Iqbal, H. M. N., Soriano, R. N. *Stem Cells and Tissue Engineering-Based Therapeutic Interventions: Promising Strategies to Improve Peripheral Nerve Regeneration*. Cell. Mol. Neurobiol. 2022, DOI: 10.1007/s10571-022-01199-3.
(65) Du, J.; Liu, J.; Yao, S.; Mao, H.; Peng, J.; Sun, X.; Cao, Z.; Yang, Y.; Xiao, B.; Wang, Y.; Tang, P.; Wang, X. Prompt peripheral nerve regeneration induced by a hierarchically aligned fibrin nanofiber hydrogel. *Acta Biomater.* **2017**, *55*, 296−309.
(66) Lopes, B.; Sousa, P.; Alvites, R.; Branquinho, M.; Sousa, A. C.; Mendonça, C.; Atayde, L. M.; Luís, A. L.; Varejão, A. S. P.; Maurício, A. C. Peripheral Nerve Injury Treatments and Advances: One Health Perspective. *Int. J. Mol. Sci.* **2022**, *23*, 918.
(67) Li, Y.; Hao, J.; Hu, Z.; Yang, Y. G.; Zhou, Q.; Sun, L.; Wu, J. Current status of clinical trials assessing mesenchymal stem cell therapy for graft versus host disease: a systematic review. *Stem Cell Res. Ther.* **2022**, *13*, 93.

https://doi.org/10.1021/acsomega.2c01176
ACS Omega 2022, 7, 18509−18520